Steel and Composite Structures, *Vol. 29, No. 3 (2018) 405-422*
DOI: https://doi.org/10.12989/scs.2018.29.3.405

Bending, buckling, and free vibration analyses of carbon nanotube reinforced composite beams and experimental tensile test to obtain the mechanical properties of nanocomposite

M. Mohammadimehr [*1], A.A. Mohammadi-Dehabadi [1,2], S.M. Akhavan Alavi [1], K. Alambeigi [1], M. Bamdad [1], R. Yazdani [1] and S. Hanifehlou [1]

[1] *Department of Solid Mechanics*, *Faculty of Mechanical Engineering*, *University of Kashan*, *Kashan*, *Iran*
[2] *Department of Mechanical Engineering*, *Iran University of Science and Technology*, *Narmak*, *Tehran*, *Iran*

(*Received November 12, 2017, Revised February 22, 2018, Accepted October 24, 2018*)

Abstract. In this research, experimental tensile test and manufacturing of carbon nanotube reinforced composite beam (CNTRC) is presented. Also, bending, buckling, and vibration analysis of CNTRC based on various beam theories such as Euler-Bernoulli, Timoshenko and Reddy beams are considered. At first, the experimental tensile tests are carried out for CNTRC and composite beams in order to obtain mechanical properties and then using Hamilton's principle the governing equations of motion are derived for Euler Bernoulli, Timoshenko and Reddy theories. The results have a good agreement with the obtained results by similar researches and it is shown that adding just two percent of carbon nanotubes increases dimensionless fundamental frequency and critical buckling load as well as decreases transverse deflection of composite beams. Also, the influences of different manufacturing processes such as hand layup and industrial methods using vacuum pump on composite properties are investigated. In these composite beams, glass fibers used in an epoxy matrix and for producing CNTRC, CNTs are applied as reinforcement particles. Applying two percent of CNTs leads to increase the mechanical properties and increases natural frequencies and critical buckling load and decreases deflection. The obtained natural frequencies and critical buckling load by theoretical method are higher than other methods, because there are some inevitable errors in industrial and hand layup method. Also, the minimum deflection occurs for theoretical methods, in bending analysis. In this study, Young's and shear modulli as well as density are obtained by experimental test and have not been used from the results of other researches. Then the theoretical analysis such as bending, buckling and vibration are considered by using the obtained mechanical properties of this research.

Keywords: bending, buckling, vibration analysis; carbon nanotube reinforced composite beam; hand layup method; industrial method using vacuum pump

1. Introduction

According to the new studies, researches have shown that composites can be achieved to better functions by adding reinforcement particles like carbon nanotubes (CNTs). Carbon nanotube reinforced composite (CNTRC) due to their superior mechanical properties such as high strength to weight ratio are widely used in different modern industries including aerospace, shipping, automobile manufacturing and civil engineering. In particular, bending, buckling, and vibration analysis is very important because these structural elements may experience different mechanical loading so analysis of CNTRC and composite considering experimental study promises new opportunities for design of high-performance mechanical systems.

Recently many investigations about composite and CNTRC materials have been done by researchers that are stated as follows:

Apuzzo *et al*. (2017) studied free vibrations of Euler-Bernoulli nano beams using stress-driven nonlocal integral model. Fundamental natural frequencies that are evaluated according to the stress-driven nonlocal integral model (SDM), are compared with results of the Eringen differential method and the gradient elasticity theory. Jin *et al*. (2016) investigated vibration and damping analysis of a sandwich beams with face sheets of laminated composite and a viscoelastic core with general boundary conditions. They also showed the effects of some parameters like layer number, ply configuration, thickness, and modulli ratios on the natural frequency and loss factor. Goncalves *et al*. (2017) worked on buckling and free vibration analysis of shear flexible sandwich beams. They created a framework to analyze free vibration and linear buckling of sandwich beams using a microstructure-dependent Timoshenko beam model. Their results demonstrated that the microstructure-dependent beam can calculate with good accuracy the natural frequencies and critical buckling loads. Emam and Nayfeh (2013) presented the non-linear response of a fixed–fixed buckled beam to a primary resonance excitation. Their results demonstrated that the first mode may or may not be activated when the third mode is directly excited. Pagani

*Corresponding author, Ph.D., Associate Professor,
E-mail: mmohammadimehr@kashanu.ac.ir

ISSN: 1229-9367 (Print), 1598-6233 (Online)

and Carrera (2017) by using Carrera unified formulation (CUF), presented governing nonlinear equations of low- to higher-order beam theories for laminated composite beams. They employed Lagrange expansion of primary variables in order to confirm kinematics description and also to provide an accurate meso-scale, beam models with independent unknowns at the layer level, in a layer-wise (LW) sense. Their numerical results for post-buckling of symmetric cross-ply beams are in a good agreement with this method. Li *et al*. (2017) considered bending, buckling and vibration analysis of an inhomogeneous beam which consist of two constituent and its properties vary through the length. Applying appropriate values of the power-law index, the mechanical behavior can be controlled. Their results showed natural frequencies and critical buckling load can be increased by increasing material length scale parameter or by decreasing nonlocal parameter. Nguyen *et al*. (2017) studied lateral buckling thin walled functionally graded (FG) beam. Using finite element method, the governing equation of equilibrium was formulated. It is concluded that buckling of thin walled FG is under control of load height level. Chen *et al*. (2017) considered nonlinear free vibration and postbuckling of FG graphene reinforced nanocomposite beams. Von kármán type nonlinearity and Timoshenko beam theory are used to obtain the governing equations. Their results showed that graphene platelets (GPLs) can effectively increase reinforcing effect on porous beams. They achieved highest beam stiffness by symmetric distribution pattern of internal pores and GPL nanofillers. Zhang *et al*. (2017) investigated the effective elastic constant of a sandwich beam with honeycomb-corrugation hybrid core by use of homogenization method. It can be concluded from the results that face sheet thickness has the greatest effect on frequency parameter and inclination angle of corrugated member does not change the frequency parameter. Gholami and Ansari (2017) studied nonlinear postbuckling of thick and moderately thick rectangular piezoelectric-piezomagnetic nanoplates with various boundary conditions under the magneto-electro-thermo-mechanical loading, their results showed that the mechanical postbuckling strength as well as critical buckling load of nanoplates are significantly influenced by the nonlocal parameter, external applied voltage and applied magnetic potential. Zhu *et al*. (2017) investigated buckling analysis of Euler–Bernoulli beams, they used nonlocal Eringen's model. Their analytical solutions confirmed that the nonlocal effect reduces the buckling loads. The nonlocal integral model that is used here has a consistent softening effect. It is also understood that the effect could be second order and first-order; it depends on the boundary conditions. Lee and Lee (2017) illustrated free vibration analysis of functionally graded beams (FGB) using an exact transfer matrix expression. This method can be applied as a great tool to obtain the mode shapes and natural frequencies for sort of problems in which material characteristics such as the elastic modulus and density are changed continuously along the height direction of the beam cross-section. Orun and Guler (2017) studied buckling analysis of thin-walled beams under combined loading. They investigated different ratios of hole diameter to reinforcement width (d/w), the aspect ratio of the web plate (a/b) and also ratios of reinforcement height to web plate thickness (h/t). Their results showed required force and energy to buckle a structure with hole reinforcement is much higher than the one without reinforcement. Piana *et al*. (2017) illustrated the natural frequencies and critical buckling load of a thin-walled open profile characterized by a slightly non-symmetric cruciform cross-section, experimentally and compared their results with numerical results. Their numerical results confirmed experimental results. Using the time-dependent boundary element method, Scuciato *et al*. (2017) presented the dynamic analysis of Euler-Bernoulli beams. Their work is based on the application of a linear θ method (or θ-Yu method), which assumes a linear time variation to the rotation, displacement, shear force and bending moment in the time interval. This version adopts linear time behavior for all variables that concerns with beam analysis in each intervals of time. Emam and Eltaher (2016) investigated the buckling and postbuckling of composite beams in hydrothermal environment. The material properties are assumed to be temperature dependent and moisture-dependent. The results depicted that the temperature has a profound contribution to the buckling and postbuckling behavior. The buckling load decreases and the postbuckling amplitude increases by increasing the temperature. Also, the moisture variation has a minimal effect on the change of the material properties, the bucking load and the postbuckling response.

Hadi and Yuan (2017) investigated experimentally on composite beams reinforced with glass fiber reinforced polymer (GFRP) I-beam and steel bars. Their proposed composite had ductile behavior because of the existence of the tensile steel bars. By replacing GFRP bars and steel bars, the brittle failure of GFRP bars caused lack of ductility of the beam and both the ultimate load and stiffness were decreased. Their results also showed that the ultimate load is controlled by the I-beam and the tensile steel bars govern the yield point of the composite beams. Zhong *et al*. (2017) studied reinforced bamboo scrimber composite (RBSC) and compared it's bending properties with un-reinforced beam. Their results proved that the reinforcement and the bamboo elements could form a composite cross-section firmly. The bending stiffness of the RBSC beams and ultimate load capacities could be improved. Types of failure: shear failure, a crack along the vertical or longitudinal direction of bamboo element. Yang *et al*. (2017) considered bending of FG nanobeams with simply supported boundary conditions based on Timoshenko beam model. They are assumed that material properties are varying along the thickness direction. Their results showed that surface stress, aspect ratio and gradient index affect the bending of FG nanobeams. With an increase in the aspect ratio, dimensionless deflection decreases. They concluded that the gradient index has more effect on deep beams than shallow ones. Gliszczyński and Kubiak (2017) investigated bending load capacity that thin walled composite beams could bear. Some results depicted that the applied failure criteria do not predict correct estimation of the maximum values of failure loads. The strength of the composite fibers is mainly defined by load capacity of the structures. Vieira *et al*.

(2017) demonstrated buckling analysis of thin-walled structures by using higher order beam models. Their obtained results of higher order beam and its comparison with FEM proved this method's efficiency and simplicity. Because the beam model considers the in-plane flexure of the cross-section, it can effectively consider local buckling. Shaat *et al*. (2016) presented the vibration characteristics of cracked nano beams made of nanocrystalline materials. They applied a size-dependent on Euler-Bernoulli beam model. It can be concluded from the results that the crack strongly influences the beam fundamental frequency when the crack is located at the fixed end of the cantilever beam where a 4.2% decrease in the frequency is obtained and the crack contribution decreases as the crack approaches the beam free end.

Bandaru *et al*. (2016) studied mechanical behavior of thermoplastic composites reinforced with two-dimensional plain woven homogeneous and hybrid fabrics of Kevlar/basalt yarns were studied. Five types of composite laminates were manufactured using compression molding technique with polypropylene (PP) resin. Static tensile and in-plane compression tests were carried out to evaluate the mechanical properties of the laminates. The tension and in-plane compression tests had shown that the composites with the combination of Kevlar and basalt yarns present better tensile and in-plane compressive behavior as compared to their base composites. Petrone and Meruane (2017) presented an investigation on the mechanical properties of a composite panel made of unidirectional flax fibres embedded in a polyethylene matrix (flax-PE). An initial set of mechanical properties was identified by classical static tests. Then, an experimental modal analysis was performed in order to get information on natural frequencies and mode shapes, which are related to the mechanical properties. Mohammadimehr and Mehrabi (2017) investigated stability and free vibration analysis of double-bonded micro composite sandwich cylindrical shells that is reinforced by CNT conveying fluid flow under mechanical load and magneto-thermo loading. Their results showed that the changes in temperature, magnetic intensity and CNT volume fraction affected on behavior of micro composite sandwich cylindrical shells. It is also can be concluded from the results that in the presence of fluid flow, the dimensionless natural frequencies reduce and as the face sheets are very stiffer than foam cores, increasing the thickness ratio leads to increase the natural frequencies and stability of micro structures. Ghorbanpour Arani *et al*. (2017b) studied nonlinear vibration behavior of viscoelastic micro composite sandwich plates which integrated with sensor and actuator. It could be concluded from the results that by applying the positive voltage to the actuator layer, frequency and stiffness of the system decreases and also with increasing the volume fraction of CNTs, the frequency of the system increases because of the increasing of the stiffness of the system. Filippi *et al*. (2014) used finite elements and various displacement theories to study static analyses of FG beams. The proposed approach can be used to study different structures such as thin plates and multilayered beams under several loadings and different boundary conditions. Arefi and Zenkour (2017a) studied vibration and magneto-electro-elastic bending analysis of a three-layer nanobeam. They used Timoshenko beam model as well as nonlocal relations to investigate the vibration and bending analysis of sandwich nanobeam integrated with piezomagnetic face sheets. Effect of some important parameters such as nonlocal parameter and applied electric and magnetic potentials on vibration and bending behavior of nanobeam was studied. Strain gradient theory of micro-structures and first-order shear deformation theory was used to investigate vibration and bending analysis of a sandwich microbeam with two integrated piezo-magnetic face-sheets by Arefi and Zenkour (2017b). Their results indicated that increasing the length scale parameters lead to increase in natural frequencies and decrease in deflection. Arefi and Zenkour (2016) presented nonlocal analysis of a sandwich nanobeam integrated with the piezomagnetic layers, using refined shear and normal deformation beam theory. Their results illustrated that parameters such as temperature rising, initial magnetic and potential and nonlocal parameter have significant effect on the bending behavior of the nanobeam. Arefi and Zenkour (2018) also, used higher-order sinusoidal shear deformation theory and strain gradient theory to derive the governing equations of electro-elastic bending of a sandwich piezoelectric microbeam resting on Pasternak's foundation. Arefi and Zenkour (2017c) investigated wave propagation, free vibration and bending analyses of a sandwich microbeam integrated with piezoelectric face-sheets resting on Pasternak foundation subjected to electric potential. They used strain gradient theory and Euler–Bernoulli beam theory to derive governing equations. They studied the effect of different parameters such as parameters of foundation, applied voltage and material length scales.

In present paper, the experimental tensile test is used to obtain the mechanical properties of carbon nanotubes reinforced composite (CNTRC) beam and theoretical bending, buckling, and vibration analysis is presented. The mechanical properties like density and Young's modulli are obtained through the experimental tests thus the accurate predictions of such composite beams can be significant research objectives. Also, in this study, the influence of different manufacturing processes such as hand layup and industrial methods by vacuum pump on composite properties is investigated. A complete analysis of bending, buckling, and vibration analysis by applying different theories such as Euler-Bernoulli, Timoshenko and Reddy is done considering different length to width ratio for both composite and nanocomposite beams. The governing equations of motion are derived for mentioned theories by using Hamilton's principle. In these composite beams, glass fiber is used in an epoxy matrix and for nanocomposite, CNTs are applied as reinforcement particles. Also, in this paper various processes are applied to produce composite beams such as hand layup and an industrial method using vacuum pump. Moreover, theoretical method of composite and nanocomposite material is considered by extended mixture and mixture rules, respectively. In this study Young's and shear modulli as well as density are obtained by experimental tensile test and the results of other researches aren't used. Then the theoretical analysis such as

bending, buckling and vibration are considered by using obtained experimental material properties.

2. Material properties

There are two methods that are used for creating composite in this study. One of them is "hand lay-up" and the other is "industrial method" which vacuum bagging is pplied.

In order to manufacture composite material in hand lay-up method, fabric layers are manually placed into the mold and the epoxy resin is applied between each layer of the glass fabric to completely coat the layer. By using a small roller, the air which are trapped, evacuated. The process is done at room temperature and no curing process is done. By uniform combining CNTs in epoxy resin and using the mixture of resin/CNT as matrix of composite, CNTRC is manufactured.

"Industrial method" is a fabricating method that uses atmospheric pressure to squeeze the resin impregnated layers together, forcing them to conform to the shape of the mold. The equipments that are used including vacuum pump, peel ply (type PA85 made by DIATEX company), sealant tape (type LSM1310 made by DIATEX company), bagging films (type PO120 made by DIATEX company), glass fabric (type CLAN AF207 made by COLAN company), epoxy resin (type EPR1080) and infusion mesh.

After lay-up is finished, the peel ply is applied over the layers to create a clean surface and over the peel ply a layer of infusion mesh is placed to assist the flow of resin across and throughout the laminate during the resin infusion process. Layers are sealed in an airtight vacuum bag and epoxy resin is transferred by force of vacuum and pass through the fabric layers. Like the previous method, the process is done at room temperature and no curing is done. Some of the advantages of this method are: no air trapped and uniform resin distribution.

Composite material has been manufactured by 11 layers glass fibers (type CLAN AF207 made by COLAN company) as well as resin epoxy (EPR 1080).

In order to determine the material properties of prototypes (composite and CNTRC beams) the Young's odulli is obtained by experimental tensile tests.

For Young's modulus test, the composite sections are cut to 90 degrees, for both without CNTs and the composite beam reinforced by two percent CNTs as shown in Figs. 1(a) and (b), respectively.

The prototypes are made by hand layup method by standard test ASTM D 3039 for tensile test which is 15 cm for its effective length and 2.5 cm for its width and 2.5 mm for its thickness. By applying Hooke's, Young's modulus can be calculated.

For shear modulus test, the specimen is inserted into the fixture according to ASTM D 3518 standard by placing two train gages element, oriented at ±45° to the loading axis, in the middle of the specimen (away from the notches) and along the loading axis, the shear response of the material can be measured.

Figs. 2(a) and (b) show the failed prototype after experimental tensile test that these composite and nanocomposite reinforced by 2% CNT beams made by hand layup method, respectively.

Figs. 3(a) and (b) depicts composite beams that are made by industrial method before and after experimental tensile test. Also Fig. 4 indicates the force versus axial deflection for prototype I1 (test 1) made by industrial method.

Table 1 shows mechanical properties including the shear modulli and Young modulli of composite beams that are made by Hand layup method.

Table 2 indicates mechanical properties such as the shear and Young modulli of carbon nanotube reinforced composite beams that are made by Hand layup method.

Table 3 illustrates mechanical properties and experimental test results such as the shear and Young modulli of composite beams that are made by industrial method.

As illustrated in Tables 1-3, there is a significant difference between Young's modulus that are obtained from hand lay-up made specimen and industrial method made specimen, that's because the process of producing. In industrial method layers are covered by resin uniformly but in hand lay-up method it could be non-uniform distribution of resin, also a high dimensional accuracy is applied in

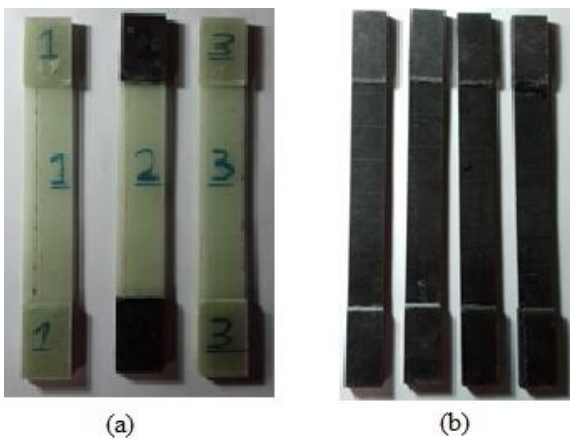

(a) (b)

Fig. 1 (a) Composite beams; (b) CNTRC beams made by hand layup method before experimental tensile test

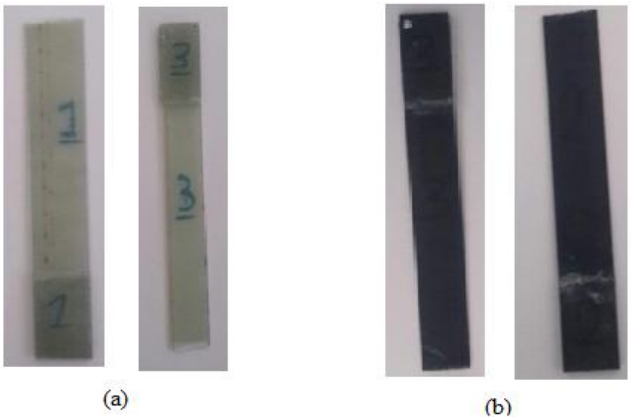

(a) (b)

Fig. 2 The failed prototype after experimental tensile test made by hand layup method (a) composite beam; (b) nanocomposite beam

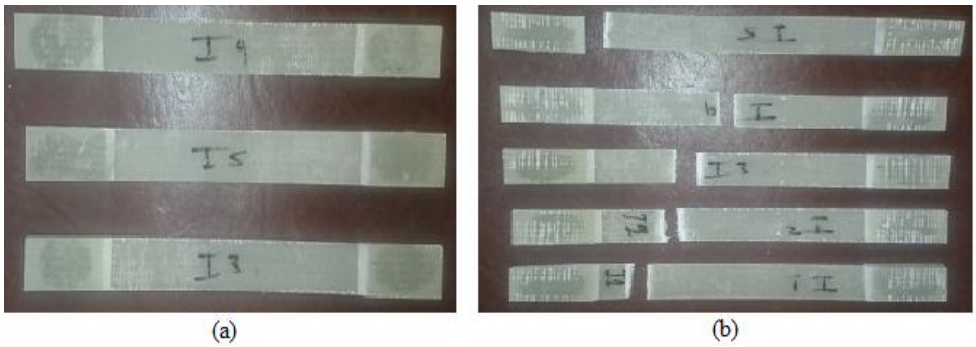

Fig. 3 Geometry of five prototypes composite beam made by industrial method (a) before experimental tensile test; (b) after experimental tensile test

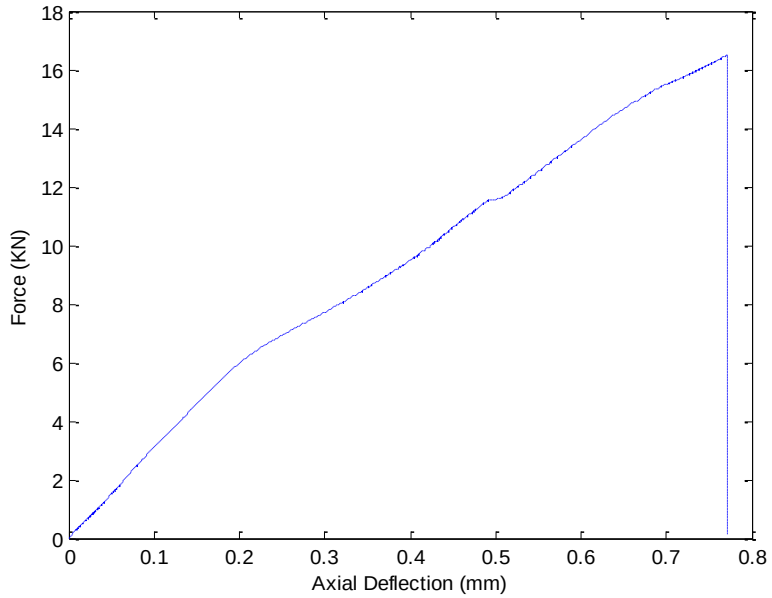

Fig. 4 Force versus axial deflection of composite beam made by industrial method for prototype I1(test 1) using Tensile test

Table 1 Mechanical properties of composite beams that are made by Hand layup method

Properties	E_{11} (GPa)	G_{12} (GPa)	ρ (kg/m^3)
Test1	7.5804	3.0815	1410
Test2	8.1745	3.3230	1410
Test3	8.1693	3.3209	1400

Table 2 Material properties of nanocomposite beams reinforced by two percentage CNT that aremade by Hand layup method

Properties	E_{11} (GPa)	G_{12} (GPa)	ρ (kg/m^3)
Test1	8.4214	3.3957	1410
Test2	8.2205	3.3147	1390
Test3	8.6104	3.4719	1400
Test4	8.5046	3.4293	1400

industrial method. Another reason related to the air trapped between layers, in industrial method vacuum pump removes the air and compress the layers over the mold to produce the beam thus the produced beam has a better quality and it causes to have better mechanical properties.

Average magnitude of mechanical properties with different methods including composite Hand layup, CNTRC hand layup and composite industrial is shown in Table 4.

In order to determine the material properties of three hase nanocomposite beam, the Halpin-Tsai equations are sed. First, the Halpin-Tsai equations are applied to obtain the mechanical properties of two-phase CNT/epoxy as matrix. The two-phase properties are then applied to compute the mechanical properties of three phase of carbon nanotube reinforced composite using the rule of mixtures. In this method, the properties of CNT/epoxy composites are used as the properties of the matrix (Sharma and Shukla 2014).

Table 3 Material properties of composite beams that are made by industrial method using vacuum pump

Properties	E_{11} (GPa)	G_{12} (GPa)	ρ (kg/m^3)	Toughness (N.m/m^3)	Critical point	Elongation (mm)	Force (KN)
I1 (Test1)	23.43	9.524	1349	720.49	Elastic limit	0.22	6.36
					Proportional limit	0.16	4.95
					Maximum stress	0.77	16.49
					Fracture	0.77	16.48
					Upper yield limit	0.31	7.82
					Lower yield limit	0.31	7.82
I2(Test2)	21.51	8.743	1342	811.47	Elastic limit	0.36	8.58
					Proportional limit	0.38	8.91
					Maximum stress	0.84	17.81
					Fracture	0.84	17.81
					Upper yield limit	0.34	8.26
					Lower yield limit	0.34	8.26
I3(Test3)	22.04	8.959	1344	539.67	Elastic limit	0.18	4.93
					Proportional limit	0.11	2.95
					Maximum stress	0.66	14.74
					Fracture	0.66	14.74
					Upper yield limit	0.27	7.03
					Lower yield limit	0.27	7.03
I4(Test4)	21.11	8.581	1341	777.43	Elastic limit	0.24	6.36
					Proportional limit	0.19	5.10
					Maximum stress	0.81	16.97
					Fracture	0.81	16.97
					Upper yield limit	0.29	7.67
					Lower yield limit	0.29	7.67
I5(Test5)	23.52	9.560	1349	608.35	Elastic limit	0.16	5.91
					Proportional limit	0.11	4.75
					Maximum stress	0.65	15.83
					Fracture	0.65	15.83
					Upper yield limit	0.21	7.10
					Lower yield limit	0.21	7.10

Table 4 Average magnitude of three type of above Tables (composite Hand layup, CNTRC hand layup and composite industrial methods)

	Composite hand layup			CNTRC hand layup			Composite Industrial method		
Properties	E_{11} (GPa)	G_{12} (GPa)	ρ (kg/m^3)	E_{11} (GPa)	G_{12} (GPa)	ρ (kg/m^3)	E_{11} (GPa)	G_{12} (GPa)	ρ (kg/m^3)
Average	7.9747	3.2418	1403	8.4392	3.4029	1400	22.322	9.0734	1345

$$E_{11}^{m}=\frac{3}{8}\left[1+2\left\{\frac{l}{d}\right\}\left\{\frac{E_{CNT}/E_{EPOXY}-\left(d/4t\right)}{E_{CNT}/E_{EPOXY}+\left(l/2t\right)}\right\}\varphi_{CNT}\right]$$
$$\times\left[1-\left\{\left\{\frac{E_{CNT}/E_{EPOXY}-\left(d/4t\right)}{E_{CNT}/E_{EPOXY}-\left(d/2t\right)}\right\}\varphi_{CNT}\right\}E_{EPOXY}\right]$$
$$+\frac{5}{8}\left[1+2\left\{\frac{E_{CNT}/E_{EPOXY}-\left(d/4t\right)}{E_{CNT}/E_{EPOXY}+\left(l/2t\right)}\right\}\varphi_{CNT}\right]$$
$$\times\left[1-\left[\left\{\frac{E_{CNT}/E_{EPOXY}-\left(d/4t\right)}{E_{CNT}/E_{EPOXY}+\left(d/2t\right)}\right\}\varphi_{CNT}\right]^{-1}E_{EPOXY}\right] \quad (1)$$

$$\varphi_{CNT}=\frac{1}{\left[\left(\rho_{CNT}/\rho_{EPOXY}\right)\times\left(M_{EPOXY}/M_{CNT}\right)\right]+1} \quad (2)$$

where E_{11}^{m}, E_{EPOXY} and E_{CNT} denote Young's modulus of matrix, epoxy and carbon nanotube and l, d, t are length, diameter and thickness of CNT respectively. φ_{CNT} is volume fraction of CNT that is given in Eq. (2).

ρ_{CNT} and ρ_{EPOXY} are density of CNT and epoxy, M_{EPOXY} is mass fraction of epoxy, and M_{CNT} is mass fraction of CNT.

V_{Fiber} and V_m are the CNT and matrix volume fractions that are written as follows

$$V_m+V_{Fiber}=1 \quad (3)$$

The Poisson's ratio is expressed as follows (Mohammadimehr *et al*. 2017)

Table 5 Material properties of CNTs (Mohammadimehr *et al*. 2016), glass fiber, and epoxy resin

Properties	E_{11} (GPa)	G_{12} (GPa)	ρ (kg/m^3)
CNT	5646.6	1944.5	1400
Glass fiber	87	29.032	1510
Epoxy resin	15.47	5.931	1100

Table 6 Geometric properties of CNTs

Diameter (nm)	Length (nm)	Thickness (nm)
30	10	2.5

$$\nu_{12} = V^{*}_{Fiber}\nu^{Fiber}_{12} + V_m\nu^m \tag{4}$$

$$V_{Fiber} = V^{*}_{Fiber} \tag{5}$$

$$V^{*}_{Fiber} = \frac{W_{Fiber}}{W_{Fiber} + \left(\frac{\rho_{Fiber}}{\rho_m}\right) - \left(\frac{\rho_{Fiber}}{\rho_m}\right)W_{Fiber}} \tag{6}$$

The mixture rule is developed for mechanical properties of fiber and matrix as follows (Mohammadimehr *et al*. 2018, Mohammadimehr and Mostafavifar 2016)

$$E_{11} = V_{Fiber}E^{Fiber}_{11} + V_mE^m_{11} \tag{7}$$

$$\rho = V_{Fiber}\rho_{Fiber} + V_m\rho_m \tag{8}$$

$$G_m = \frac{E_m}{2(1+\nu)} \tag{9}$$

where E_{11}, G_{12} and ρ denote Young modulus, shear and density coefficients, respectively.

Also, Table 5 shows the material properties including Young's and shear modulli as well as density of CNTs, glass fiber, and epoxy resin.

Geometric properties of CNTs including length, thickness and diameter are shown in Table 6.

Comparison between theoretical and experimental results of a beam made by hand lay-up method is presented in Table 7.

Substituting the material properties from Tables 5 and 6 in Eqs. (1)-(9) and using Halpin-Tsai and a comparison of experimental and the theoretical results of Young's and shear modulli as well as density for a nanocomposite beam made by hand layup method is presented in Table 8. Also using mixture rule a comparison of experimental and the theoretical results of Young's and shear modulli as well as density for a composite beam made by an industrial method using vacuum pump is shown in Table 9. The volume fraction of fiber and epoxy resin are 37 and 63 percent, respectively.

In Tables 7 and 8 show a remarkable difference between theoretical and experimental amount, the reasons of this are non-uniform distribution of resin in hand lay-up method, and air trapped between layers. Theoretical results are obtained by considering the ideal condition, that means there is no error in producing process that's why it has the highest amount of Young's modulus; while in Table 9, theoretical and experimental results of Young's and shear modulli and density for a composite beam made of industrial method are compared that it is shown the difference between two methods is lower than Tables 7 and 8. In "Industrial method" is a fabricating method that uses atmospheric pressure to squeeze the resin impregnated layers together, forcing them to conform to the shape of the mold. Thus, in this method, layers are sealed in an airtight

Table 7 Comparing theoretical and experimental results of Young's and shear modulli and density for a composite beam made by hand layup

	Theory			Experimental test		
Properties	E_{11} (GPa)	G_{12} (GPa)	ρ (kg/m^3)	E_{11} (GPa)	G_{12} (GPa)	ρ (kg/m^3)
	23.0376	9.3649	1272	7.9747	3.2418	1403

Table 8 Comparing theoretical and experimental results of Young's and shear modulli and density for a carbon nanotube reinforced composite beam made by hand layup method

	Theory			Experimental test		
Properties	E_{11} (GPa)	G_{12} (GPa)	ρ (kg/m^3)	E_{11} (GPa)	G_{12} (GPa)	ρ (kg/m^3)
	36.41	14.00	1274	8.4392	3.4029	1400

Table 9 Comparing theoretical and experimental results of Young's and shear modulli and density for a composite beam made by industrial method

	Theory			Experimental test		
Properties	E_{11} (GPa)	G_{12} (GPa)	ρ (kg/m^3)	E_{11} (GPa)	G_{12} (GPa)	ρ (kg/m^3)
	23.0376	9.3649	1272	22.322	9.0734	1345

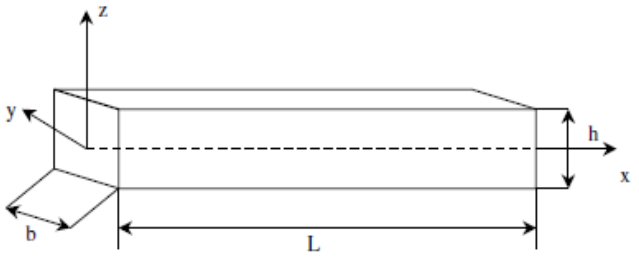

Fig. 5 Geometry of composite beam and coordinate system

vacuum bag and epoxy resin is transferred by force of vacuum and pass through the fabric layers. Like the previous method, the process is done at room temperature and no curing is done. Some of the advantages of this method are: no air trapped and uniform resin distribution.

3. Mathematical formulation

A straight uniform composite beam is shown in Fig. 5. As it can be seen *b*, *L* and *h* are thickness, length and width of the beam. In this beam deformation occurs at *x*-*z* plane and the deformation in the y direction is neglected in this approach.

The normal and shear stresses of the composite beam by the generalized Hooke's law are stated as follows (Goswami and Becker 2015, Arani *et al*. 2017a)

$$\begin{Bmatrix}\sigma_x\\ \tau_{xz}\end{Bmatrix}=\begin{bmatrix}Q_{11} & 0\\ 0 & Q_{22}\end{bmatrix}\begin{Bmatrix}\varepsilon_x\\ \gamma_{xz}\end{Bmatrix} \tag{10}$$

$$Q_{11}=\frac{E_{11}}{1-\nu_{12}\nu_{21}} \tag{11}$$

$$Q_{22}=G \tag{12}$$

In this study, displacement fields for the composite beam along the *x*, *y* and *z* direction are *u*, *v* and *w* that for high order composite beam are defined as follows (Mohammadimehr *et al*. 2016)

$$\begin{aligned}u(x,y,z,t)&=u_0(x,t)-\alpha_1\, z\,\frac{\partial w_0(x,t)}{\partial x}\\ &+\alpha_2\, z\,\psi(x,t)+\alpha_3\frac{-4z^3}{3h^2}\left(\psi(x,t)+\frac{\partial w_0(x,t)}{\partial x}\right)\\ v(x,y,z,t)&=0\\ w(x,y,z,t)&=w_0(x,t)\end{aligned} \tag{13}$$

In this displacement fields, if $\alpha_2 = 0$, $\alpha_1 = \alpha_3 = 0$ and $\alpha_2 = \alpha_3 = 0$ the Reddy, Timoshenko and Euler-Bernoulli theories are obtained.

The strain-displacement relation for the composite beam is considered as follows (Xu *et al*. 2017, Wattanasakulpong *et al*. 2012, Mohammadimehr and Shahedi 2016)

$$\begin{aligned}\varepsilon_x&=\frac{\partial u}{\partial x},\qquad \varepsilon_y=\frac{\partial v}{\partial y}=0,\\ \varepsilon_z&=\frac{\partial w_0}{\partial z}=0,\qquad \gamma_{xz}=\frac{\partial u}{\partial z}+\frac{\partial w}{\partial x}\end{aligned} \tag{14}$$

3.1 The kinematic equations for composite beam

Substituting Eq. (13) into Eq. (14), the kinematic equations for high order composite beam are obtained as follows (Nayak *et al*. 2002, Zamani *et al*. 2014, Mohammadimehr *et al*. 2016).

$$\begin{aligned}\varepsilon_x&=\frac{\partial u_0(x,t)}{\partial x}-\alpha_1 z\,\frac{\partial^2 w_0(x,t)}{\partial x^2}+\alpha_2 z\,\frac{\partial \psi(x,t)}{\partial x}\\ &+\alpha_3\frac{-4z^3}{3h^2}\left(\frac{\partial \psi(x,t)}{\partial x}+\frac{\partial^2 w(x,t)}{\partial x^2}\right)\end{aligned} \tag{15}$$

$$\varepsilon_z=\frac{\partial w_0(x,t)}{\partial z} \tag{16}$$

$$\begin{aligned}\gamma_{xz}&=\frac{\partial u_0(x,t)}{\partial z}-\alpha_1\left(\frac{\partial w_0(x,t)}{\partial x}+z\,\frac{\partial^2 w_0(x,t)}{\partial x\,\partial z}\right)\\ &+\alpha_2\left(\psi(x,t)+z\,\frac{\partial \psi(x,t)}{\partial z}\right)\\ &+\alpha_3\left(\frac{-12z^2}{3h^2}\right)\left(\psi(x,t)+\frac{\partial w_0(x,t)}{\partial x}\right)+\frac{\partial w_0(x,t)}{\partial x}\end{aligned} \tag{17}$$

To simplify the above equations ε_x^0, k_x, k'_x, k_{xz}, γ_{xz}^0 and k'_{xz} are defined as follows

$$\varepsilon_x^0=\frac{\partial u_0(x,t)}{\partial x} \tag{18}$$

$$k_x=-\alpha_1\frac{\partial^2 w_0(x,t)}{\partial x^2}+\alpha_2\frac{\partial \psi(x,t)}{\partial x} \tag{19}$$

$$k'_x=-\alpha_3\frac{4}{3h^2}\left(\frac{\partial \psi(x,t)}{\partial x}+\frac{\partial^2 w(x,t)}{\partial x^2}\right) \tag{20}$$

$$k_{xz}=-\alpha_3\frac{4}{h^2}\left(\psi(x,t)+\frac{\partial w_0(x,t)}{\partial x}\right) \tag{21}$$

$$\gamma_{xz}^0=-\alpha_1\frac{\partial w_0(x,t)}{\partial x} \tag{22}$$

$$k'_{xz}=-\alpha_1\frac{\partial^2 w_0(x,t)}{\partial x\,\partial z}=0 \tag{23}$$

By substituting Eqs. (18)-(23) into Eqs. (15)-(17) are simplified as follows

$$\varepsilon_x=\varepsilon_x^0+zk_x+z^3k'_x \tag{24}$$

$$\varepsilon_z = \varepsilon_z^0 = \frac{\partial w_0(x,t)}{\partial z} = 0 \tag{25}$$

$$\gamma_{xz} = \gamma_{xz}^0 + zk'_{xz} + z^2 k_{xz} \tag{26}$$

3.2 Hamilton's principle.

The total potential energy is written as follows Fereidoon *et al*. (2015)

$$\Pi = T - (U + W) \tag{27}$$

where *T*, *U* and *W* are the kinetic energy, the strain energy and the work done due to the external force, respectively; in this study external force for the vibration analysis of the composite beam is equal to zero.

The variation of kinetic energy is considered as follows (Ansari *et al*. 2017, Ebrahimi and Barati 2017, Arefi 2015)

$$\delta T = \int_{\forall} \rho(\dot{u}\,\delta\dot{u} + \dot{v}\,\delta\dot{v} + \dot{w}\,\delta\dot{w})dV \tag{28}$$

where ρ is the density of the composite beam and $\dot{u}$, $\dot{v}$, $\dot{w}$ are the velocities of the composite beam in *x*, *y* and *z* directions, respectively; *V* is the volume of the beam.

Substituting Eq. (13) into Eq. (28) is obtained the following equation

$$\begin{aligned}
T = \int_0^l \Bigg(& \left(\int_{-0.5h}^{0.5h} \rho(z)dz \right)(u_{tt}(x,t)\delta u_0(x,t) \\
& - w_{tt}(x,t)\delta w_0(x,t)) + \left(\int_{-0.5h}^{0.5h} \rho(z) z^3 dz \right) \\
& \left(\frac{4}{3}\frac{\alpha_3 w_{xtt}(x,t)\delta u_0(x,t)}{h^2} + \frac{4}{3}\frac{\alpha_3 u_{tt}(x,t)\delta\psi_0(x,t)}{h^2} \right. \\
& \left. - \frac{4}{3}\frac{\alpha_3 u_{xtt}(x,t)\delta w_0(x,t)}{h^2} + \frac{4}{3}\frac{\alpha_3 \psi_{tt}(x,t)\delta u_0(x,t)}{h^2} \right) \\
& + \left(\int_{-0.5h}^{0.5h} \rho(z) z^2 dz \right)\Big(\alpha_1\alpha_2 w_{xtt}(x,t)\delta\psi_0(x,t) \\
& - \alpha_1\alpha_2\psi_{xtt}(x,t)\delta w_0(x,t) + \alpha_1^2 w_{xxtt}(x,t)\delta w_0(x,t) \\
& - \alpha_2^2\psi_{tt}(x,t)\delta\psi_0(x,t)\Big) + \left(\int_{-0.5h}^{0.5h} \rho(z) z dz \right) \\
& \big(-\alpha_1 u_{xtt}(x,t)\delta w_0(x,t) - \alpha_2 u_{tt}(x,t)\delta\psi_0(x,t) \\
& + \alpha_1 w_{xtt}(x,t)\delta u_0(x,t) \\
& - \alpha_2\psi_{tt}(x,t)\delta u_0(x,t)) + \left(\int_{-0.5h}^{0.5h} \rho(z) z^4 dz \right) \\
& \left(-\frac{4}{3}\frac{\alpha_1\alpha_3 w_{xtt}(x,t)\delta\psi_0(x,t)}{h^2} + \frac{8}{3}\frac{\alpha_1\alpha_3 w_{xxtt}(x,t)\delta w_0(x,t)}{h^2} \right. \\
& + \frac{8}{3}\frac{\alpha_2\alpha_3\psi_{tt}(x,t)\delta\psi_0(x,t)}{h^2} - \frac{4}{3}\frac{\alpha_2\alpha_3\psi_{xtt}(x,t)\delta w_0(x,t)}{h^2} \\
& \left. + \frac{4}{3}\frac{\alpha_1\alpha_3\psi_{xtt}(x,t)\delta w_0(x,t)}{h^2} + \frac{4}{3}\frac{\alpha_2\alpha_3 w_{xtt}(x,t)\delta\psi_0(x,t)}{h^2} \right) \\
& + \left(\int_{-0.5h}^{0.5h} \rho(z) z^4 dz \right)\left(-\frac{16}{9}\frac{\alpha_3^2 w_{xtt}(x,t)\delta\psi_0(x,t)}{h^4} \right. \\
& + \frac{16}{9}\frac{\alpha_3^2 w_{xxtt}(x,t)\delta w_0(x,t)}{h^4} - \frac{16}{9}\frac{\alpha_3^2\psi_{tt}(x,t)\delta\psi_0(x,t)}{h^4} \\
& \left. + \frac{16}{9}\frac{\alpha_3^2\psi_{xtt}(x,t)\delta w_0(x,t)}{h^4} \right) \Bigg) dx
\end{aligned} \tag{29}$$

$$\delta U = \int_{\forall} \left(\sigma_x\,\delta\varepsilon_x + \tau_{xz}\,\delta\gamma_{xz} \right) dxdydz \tag{30}$$

where *U* is strain energy (Shao *et al*.2017, Ganapathi *et al*.2017); σ_x and τ_{xz} are the normal and shear stresses and ε_x, and γ_{xz} denote normal, shear strains, respectively.

By substituting Eqs. (10), (24), (25) and (26) into Eq. (31) yields the following relation

$$\begin{aligned}
\delta U = \int_{\forall} \Big(& \left(Q_{11}\left(\varepsilon_x^0 + zk_x + z^3 k'_x \right)\left(\delta\varepsilon_x^0 + z\,\delta k_x + z^3\delta k'_x \right) \right. \\
& \left. + Q_{22}\left(\gamma_{xz}^0 + z^2 k_{xz} \right)\left(\delta\gamma_{xz}^0 + z^2\delta k_{xz} \right) \right) dxdydz
\end{aligned} \tag{31}$$

By solving the relation (31), the strain energy is obtained as follows

$$\begin{aligned}
\delta U = \int_0^l \Bigg(& -u_{xx}(x,t)\delta u_0(x,t)\left(\int_{-0.5h}^{0.5h} Q_{22}(z)dz \right) \\
& + \left(-\alpha_1 u_{xxx}(x,t)\delta w_0(x,t) - \alpha_2 u_{xx}(x,t)\delta\psi_0(x,t) \right. \\
& \left. + \alpha_1 w_{xxx}(x,t)\delta u_0(x,t) - \alpha_2\psi_{xx}(x,t)\delta u_0(x,t) \right) \\
& \left(\int_{-0.5h}^{0.5h} Q_{11}(z)zdz \right) + \left(\alpha_1\alpha_2 w_{xxx}(x,t)\delta\psi_0(x,t) \right. \\
& - \alpha_1\alpha_2\psi_{xxx}(x,t)\delta w_0(x,t) + \alpha_1^2 w_{xxxx}(x,t)\delta w_0(x,t) \\
& \left. - \alpha_2^2\psi_{xx}(x,t)\delta\psi_0(x,t) \right)\left(\int_{-0.5h}^{0.5h} Q_{22}(z) z^2 d \right. \\
& + \left(\frac{4}{3}\frac{\alpha_3 u_{xx}(x,t)\delta\psi_0(x,t)}{h^2} - \frac{4}{3}\frac{\alpha_3 u_{xxx}(x,t)\delta w_0(x,t)}{h^2} \right. \\
& \left. + \frac{4}{3}\frac{\alpha_3\psi_{xx}(x,t)\delta u_0(x,t)}{h^2} \right. \\
& \left. + \frac{4}{3}\frac{\alpha_3 w_{xxx}(x,t)\delta u_0(x,t)}{h^2} \right)\left(\int_{-0.5h}^{0.5h} Q_{11}(z) z^3 dz \right) \\
& + \left(-\frac{4}{3}\frac{\alpha_1\alpha_3 w_{xxx}(x,t)\delta\psi_0(x,t)}{h^2} \right. \\
& + \frac{8}{3}\frac{\alpha_1\alpha_3 w_{xxxx}(x,t)\delta w_0(x,t)}{h^2} + \frac{8}{3}\frac{\alpha_2\alpha_3\psi_{xx}(x,t)\delta\psi_0(x,t)}{h^2} \\
& - \frac{4}{3}\frac{\alpha_2\alpha_3\psi_{xxx}(x,t)\delta w_0(x,t)}{h^2} \\
& \left. + \frac{4}{3}\frac{\alpha_1\alpha_3\psi_{xxx}(x,t)\delta w_0(x,t)}{h^2} + \frac{4}{3}\frac{\alpha_2\alpha_3 w_{xxx}(x,t)\delta\psi_0(x,t)}{h^2} \right) \Bigg| \\
& \left(\int_{-0.5h}^{0.5h} Q_{22}(z) z^4 dz \right)
\end{aligned} \tag{32}$$

Table 10 Dimensionless fundamental natural frequency of an isotropic beam for three theories by the present work and Koochaki (2011) $\Omega = \Omega^* l^2 (\frac{\rho}{E_2})^{0.5} / h$

h/*L*	0.01	0.0125	0.025	0.05	0.1
Euler-Bernoulli	2.985526	2.985232	2.982588	2.971688	2.931568
Euler-Bernoulli (present work)	2.986555	2.986486	2.985910	2.983612	2.974471
FSDT	2.986137	2.985827	2.983285	2.973193	2.934044
Timoshenko (present work)	2.986204	2.985938	2.983722	2.974922	2.940669
TSDT	2.9861380	2.9858280	2.9832858	2.9731941	2.9340570
Reddy (present work)	2.9861344	2.9858287	2.9832858	2.9731942	2.9340576

Table 11 Non-dimensional central deflection, $W(0.5) \times 10^{-3}$ for different values of *k* (power index of FGM) and $l/h = 5$ using the obtained results by present work and (Li *et al*.2013) $(W = \frac{w_0}{l})$

k	0	0.5	10	100	10^{11}
Li *et al*. (2013) (Method-1)	2.6252	4.0113	8.8830	12.792	14.251
Li *et al*. (2013) (Method-2)	2.3986	3.7001	8.0060	11.614	13.021
Present work	2.6935	3.8998	8.5327	13.106	14.622

$$
\begin{aligned}
&+\left(-\frac{16}{9}\frac{\alpha_3^2 w_{xxx}(x,t)\delta\psi_0(x,t)}{h^4}+\frac{16}{9}\frac{\alpha_3^2 w_{xxxx}(x,t)\delta w_0(x,t)}{h^4}\right.\\
&-\frac{16}{9}\frac{\alpha_3^2 \psi_{xx}(x,t)\delta\psi_0(x,t)}{h^4}\\
&\left.+\frac{16}{9}\frac{\alpha_3^2 \psi_{xxx}(x,t)\delta w_0(x,t)}{h^4}\right)B_5\Big)tdx\\
&+\int_0^l\Big(\big(\alpha_1\alpha_2\psi_x(x,t)\delta w_0(x,t)\\
&-\alpha_1^2 w_{xx}(x,t)\delta w_0(x,t)+\alpha_2^2\psi(x,t)\delta\psi_0(x,t)\\
&-\alpha_2\psi_x(x,t)\delta w_0(x,t)+2\alpha_1 w_{xx}(x,t)\delta w_0(x,t)\\
&-\alpha_1\alpha_2 w_x(x,t)\delta\psi_0(x,t)-w_{xx}(x,t)\delta w_0(x,t)\\
&+\alpha_2 w_x(x,t)\delta\psi_0(x,t)\big)\left(\int_{-0.5h}^{0.5h}Q_{22}(z)dz\right)\\
&+\left(-\frac{8\alpha_2\alpha_3\psi(x,t)\delta\psi_0(x,t)}{h^2}-\frac{4\alpha_2\alpha_3 w_x(x,t)\delta\psi_0(x,t)}{h^2}\right.\\
&+\frac{4\alpha_3\psi_x(x,t)\delta w_0(x,t)}{h^2}\\
&-\frac{8\alpha_1\alpha_3 w_{xx}(x,t)\delta w_0(x,t)}{h^2}+\frac{4\alpha_2\psi_x(x,t)\delta w_0(x,t)}{h^2}\\
&\left.-\frac{4\alpha_1\alpha_3\psi_x(x,t)\delta w_0(x,t)}{h^2}\right)\left(\int_{-0.5h}^{0.5h}Q_{22}(z)z^2dz\right)\\
&+\left(\frac{16\alpha_3^2\psi(x,t)\delta\psi_0(x,t)}{h^4}-\frac{16\alpha_3^2\psi_x(x,t)\delta w_0(x,t)}{h^4}\right.\\
&+\frac{16\alpha_3^2 w_x(x,t)\delta\psi_0(x,t)}{h^4}\\
&\left.-\frac{16\alpha_3^2 w_{xx}(x,t)\delta w_0(x,t)}{h^4}\right)\left(\int_{-0.5h}^{0.5h}Q_{22}(z)z^4dz\right)
\end{aligned}
\tag{32}
$$

$$\delta W = -\int_0^1 \big(f_z(x)\delta w_0(x,t)\big)dx \tag{33}$$

where *W* is external work and *f* is external force (Jacob *et al*. 2002)

By substituting the Eqs. (29), (32) and (33) in the Hamilton's principle, the equations of the motion for the CNTRC beam are completely defined in Appendix A.

To solve the governing equations of motion, the Navier's solution is defined as follows (Mohammadimehr *et al*. 2015, Ganapathi and Polit 2017, Naderi *et al*. 2014, Mehrabian *et al*. 2005)

$$u_0(x,t) = \sum_{n=1}^{\infty} U_0 \cos\frac{n\pi x}{l}e^{i\omega t} \tag{34}$$

$$\psi(x,t) = \sum_{n=1}^{\infty} \Psi_0 \cos\frac{n\pi x}{l}e^{i\omega t} \tag{35}$$

$$w_0(x,t) = \sum_{n=1}^{\infty} W_0 \sin\frac{n\pi x}{l}e^{i\omega t} \tag{36}$$

4. Validation

For validation of this study, the results are compared with other researches. In order to achieve this purpose, dimensionless fundamental natural frequency of a beam is compared with the obtained results by the references Koochaki (2011). The material properties are assumed as follows Koochaki (2011)

$$
\begin{aligned}
&E_1 = 380(G\,\text{Pa}),\ E_2 = 70(G\,\text{Pa})\\
&v_1 = 0.3,\ v_2 = 0.3, k = 0\\
&\rho_1 = 3800(kg/m^3),\ \rho_2 = 2707(kg/m^3)
\end{aligned}
\tag{37}
$$

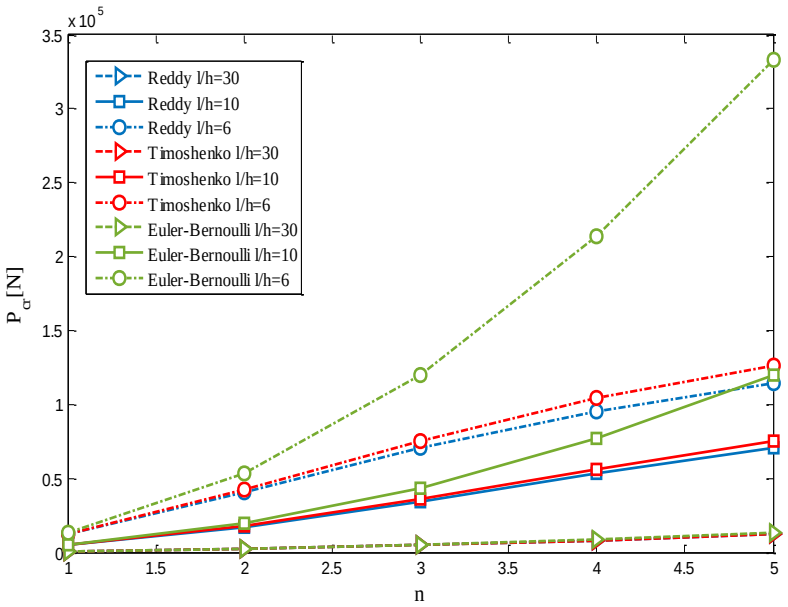

Fig. 6The critical buckling loads of CNTRC beams in various length to thickness ratio and axial wave numbers. (l = 1 m)

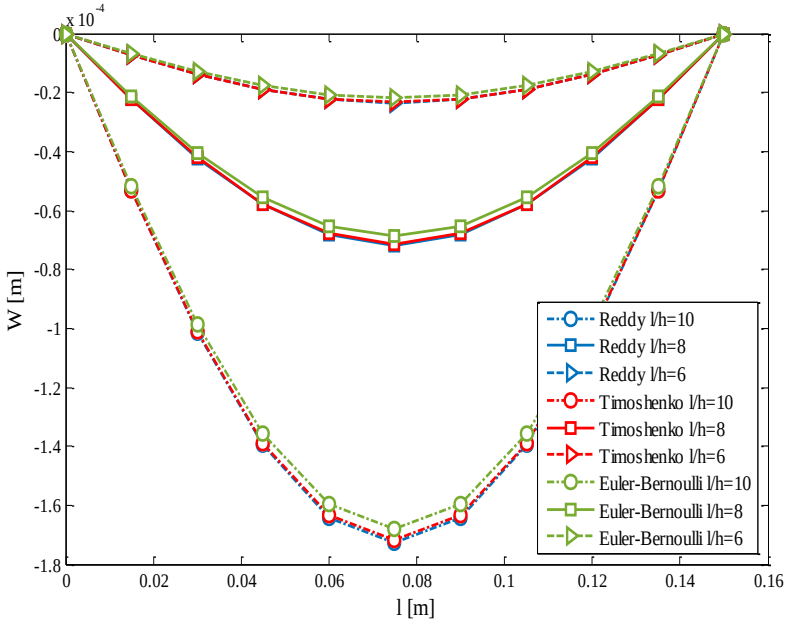

Fig. 7 The deflections of nanocomposite beams in various length to thickness ratio

The dimensionless fundamental natural frequency by the present work for three theories (Euler-Bernoulli, Timoshenko and Reddy beam models) are compared with the presented results by Koochaki (2011) for various theories (Euler-Bernoulli, first-order shear deformation theory (FSDT), third-order shear deformation theory (TSDT)) in Table 10. It is shown that the present work and the obtained results by Koochaki (2011) have a good agreement together for isotropic materials.

Table 11 shows non-dimensional central deflection, W (0.5) × 10^{-3} for different values of k (power index of FGM) and l/h = 5 using the obtained results by present work and Li *et al*. (2013) that have a good agreement with each other.

5. Numerical results

In this article, bending, buckling, and vibration analysis of high order nanocomposite beam based on experimental study is investigated. At first, the experimental tensile tests carried out in order to obtain mechanical properties such as density, shear and Young's modulli and then using Hamilton's principle the governing equations of motion have been derived for Euler Bernoulli, Timoshenko and Ready theories. In this composite, glass fibers have been used in epoxy matrix and for nanocomposite, CNTs have been used as reinforcement particles by uniform distribution.

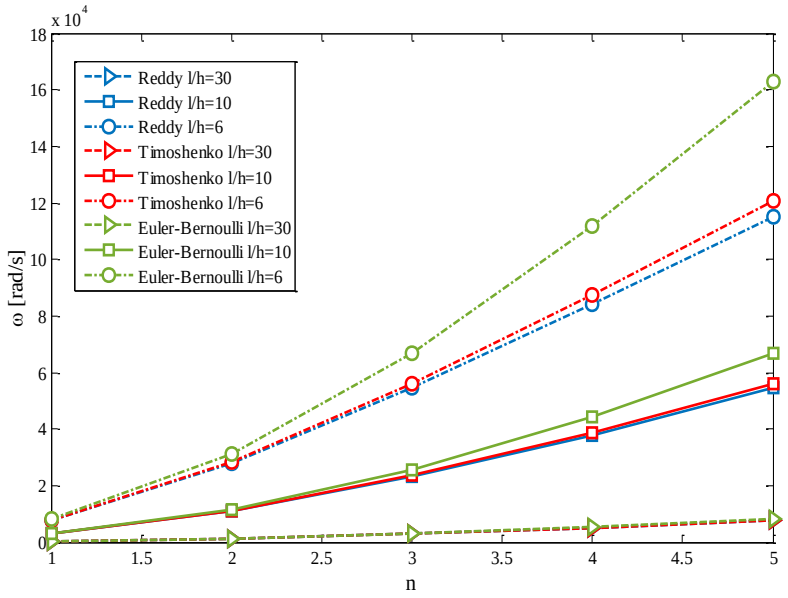

Fig. 8 The natural frequencies of CNTRC beams in various length to thickness ratio and modes

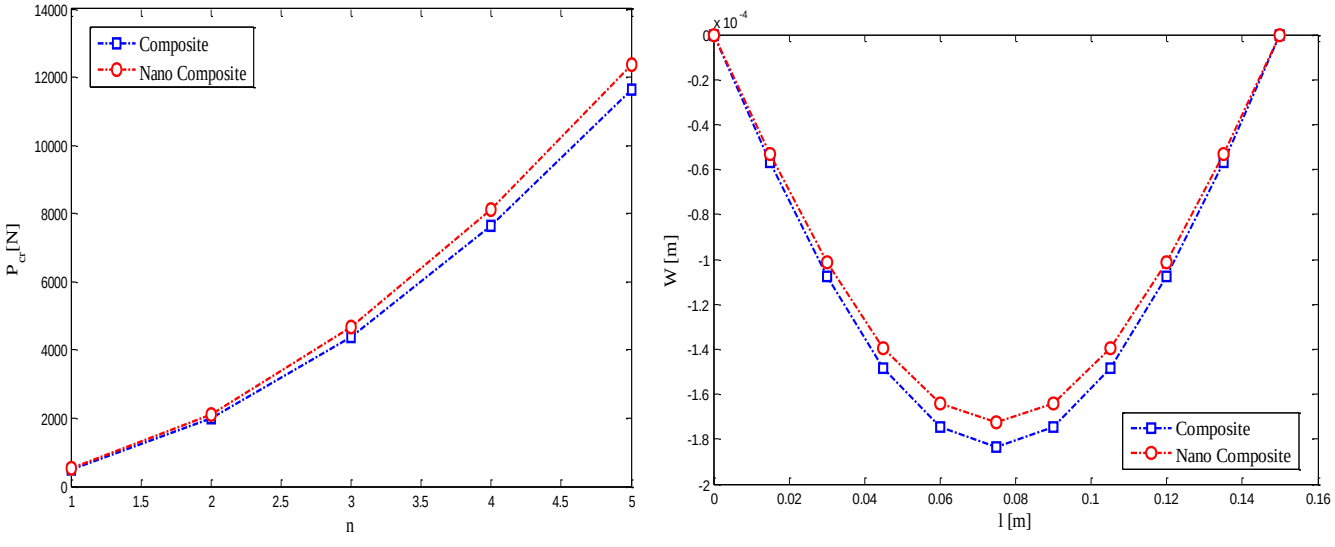

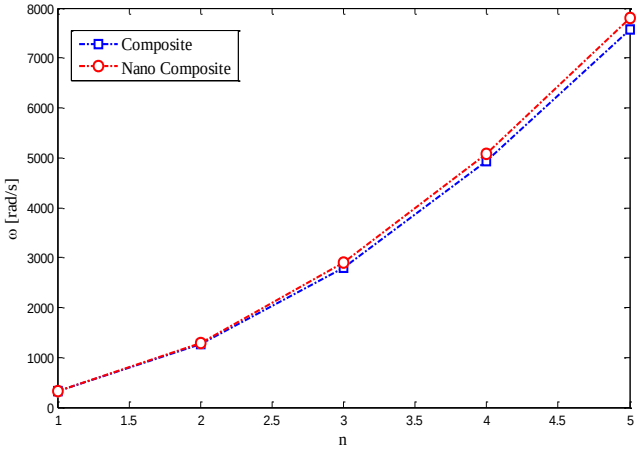

Fig. 9 The effect of adding two percent of CNTs in composite as reinforcement particles on (a) critical buckling load l/h = 30; (b) deflection of beam l/h = 10; and (c) natural frequencies l/h = 10

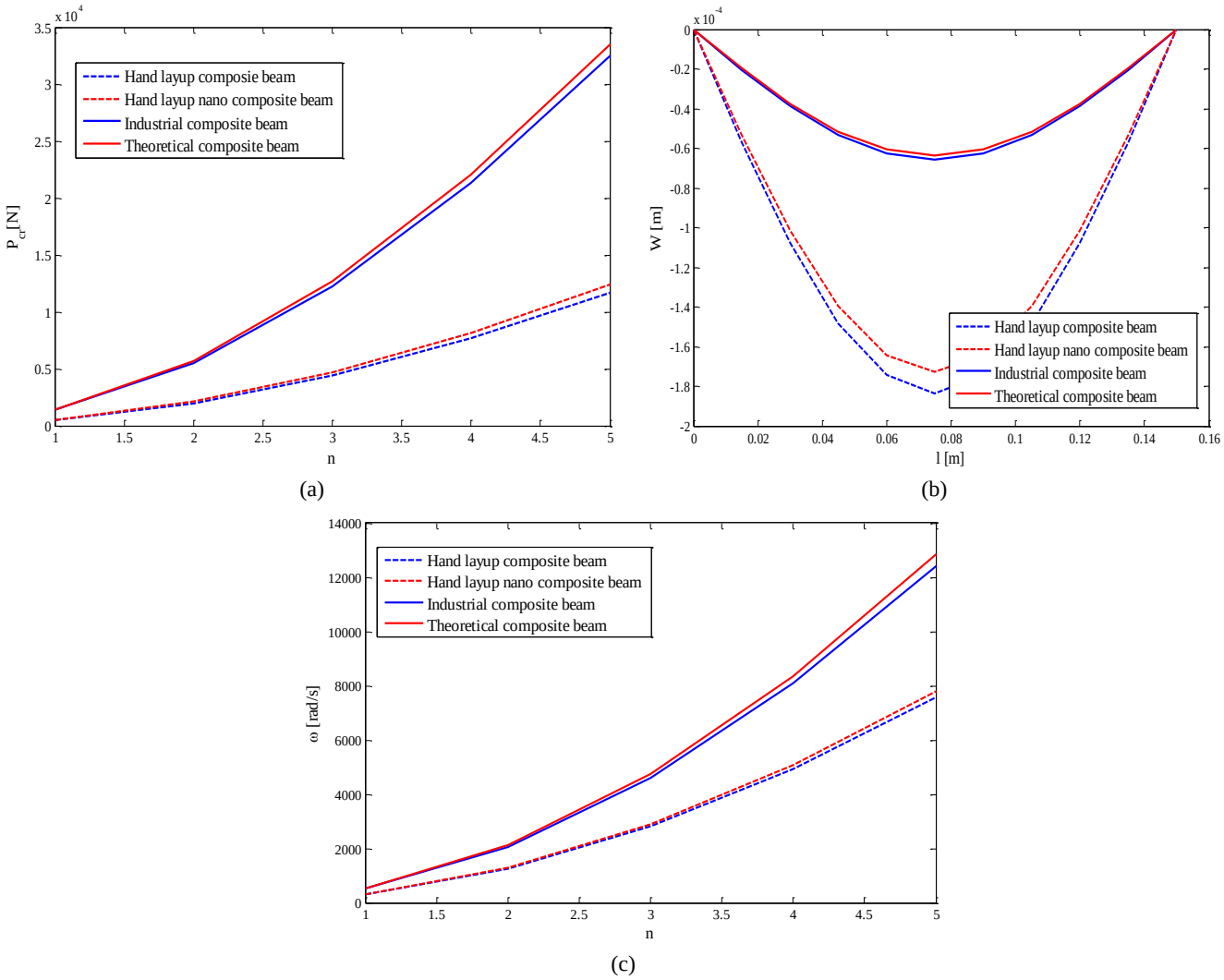

Fig. 10 The influence of applying various processes such as hand layup, industrial and theoretical methods on (a) critical buckling load l/h = 30; (b) deflection of beam l/h = 10; and (c) natural frequencies l/h = 10

Also, the mechanical properties of composite and CNTRC materials are illustrated in Table 4 made by hand layup method.

Fig. 6 shows the critical buckling loads of CNTRC beams in various length to thickness ratio and wave axial numbers as well as considering different beam theories such as Euler-Bernoulli, Timoshenko and Reddy. By increasing axial wave numbers (mode numbers) and decreasing length to thickness ratio the effect of considering more accurate theories and critical buckling load increase. Also, the critical buckling load for Euler-Bernoulli theory is higher than that of for other theories. Thus, Timoshenko and Reddy beam theories are softer than Euler-Bernoulli beam theory. Also, for high aspect ratio (length to thickness ratio) the obtained results by three beam theories are similar together.

Using the obtained result made by hand layup method in Table 4, Figs. 7-10 have been plotted.

Fig. 7 illustrates the deflections of CNTRC beams in various length to thickness ratio by considering different beam theories. The effect of considering various theories is more significant in the central of the beam and Reddy and Euler-Bernoulli beam theories result maximum and minimum deflections, respectively. Increasing length to thickness ratio leads to increase the central deflection. Also increasing the aspect ratio, the effect of considering more accurate theory enhances.

Fig. 8 depicts the natural frequencies of CNTRC beams in various length to thickness ratio and modes as well as different theories. By decreasing length to thickness ratio and increasing axial wave numbers (mode numbers) the influence of investigating more accurate theory and natural frequencies increase. Also, Reddy and Euler-Bernoulli theories result maximum and minimum natural frequencies respectively.

According to Figs. 6-8, the influence of considering more accurate theory is more significant for buckling and vibration analysis rather than deflection.

Figs. 9(a), (b), and (c) show the effect of adding two percent of CNTs as reinforcement particles inside composite matrix based on Reddy beam theory. Considering CNTs leads to increase the mechanical properties and increases natural frequencies and critical buckling load and decreases deflection. It can be seen that the stiffness of the

carbon nanotube reinforced composite is higher than that of composite structure which leads to enhance the natural frequencies and critical buckling load and vice versa for transverse deflection.

The influence of applying various processes such as hand layup, industrial and theoretical methods on critical buckling load, deflection of beam and natural frequencies is shown in Figs. 10(a), (b) and (c). According to Figs. 10(a) and (c), the natural frequencies and critical buckling load of theoretical method are higher than other methods and vice versa for deflection of beam in Fig. 10(b) because for industrial and hand layup method we cannot made a perfect composite beam with one hundred percent agreement by theoretical investigation. Also, it is shown from this figures that the results for industrial method by vacuum pump is higher than that of hand layup method, because the composite structure made by industrial method has the minimum vacancy with respect to hand layup method.

Also Fig. 10(b) shows that the minimum deflection occurs for theoretical methods, in bending analysis.

It can be seen that the obtained results by theoretical (Reddy) composite beam and industrial composite beam are near to each other; while these results are different from the hand layup for composite and CNTRC beam. The reasons of these results are non-uniform distribution of resin in hand lay-up method, and air trapped between layers. Theoretical results are obtained by considering the ideal condition (Halpin-Tsai as well as rule of mixture), that means there is no error is occurred in producing process that's why it has the highest amount of Young's modulus; while in Table 9, theoretical and experimental results of Young's and shear modulli and density for a composite beam made of industrial method are compared that it is shown the difference between two methods is lower than Tables 7 and 8. In "Industrial method" is a fabricating method that uses atmospheric pressure to squeeze the resin impregnated layers together, forcing them to conform to the shape of the mold. Thus, in this method, layers are sealed in an airtight vacuum bag and epoxy resin is transferred by force of vacuum and pass through the fabric layers. Like the previous method, the process is done at room temperature and no curing is done. Some of the advantages of this method are: no air trapped and uniform resin distribution.

As can be seen, in this case, the influence of applying more accurate processes to produce composite structures is more important than adding nano reinforcement particles.

6. Conclusions

In this article, the experimental tensile tests carried out in order to obtain mechanical properties of composite and CNTRC beam such as density, shear and Young's modulli. Then, using these properties, bending, buckling, and vibration analysis of nanocomposite beam is investigated, also, by using Hamilton's principle the governing equations of motion for Euler Bernoulli, Timoshenko and Reddy theories are derived. In these composite beams, glass fiber is used in an epoxy matrix and for CNTRC, CNTs are applied as reinforcement particles. Also, in this paper various processes are applied to produce composite beams such as hand layup and an industrial method using vacuum pump. Moreover, theoretical method of composite and nanocomposite material is considered by extended mixture and mixture rules, respectively.

Some obtained results of present research are stated as follows:

(1) By increasing axial wave numbers (mode numbers) and decreasing length to thickness ratio, the effect of considering more accurate theories, the natural frequency and critical buckling load increase. Also, the critical buckling load for Euler-Bernoulli theory is higher than that of for other theories. Thus, it is concluded that Timoshenko and Reddy beam theories are softer than Euler-Bernoulli beam theory. Also, for high aspect ratio (length to thickness ratio) the obtained results by three beam theories are similar to each other.
(2) The effect of considering various theories is more significant in the central of the beam and Reddy and Euler-Bernoulli beam theories result maximum and minimum deflections, respectively. Increasing aspect ratio leads to increase the deflection.
(3) The influence of considering more accurate theory is more significant for buckling and vibration analysis rather than bending.
(4) Employing two percent of CNTs leads to increase the mechanical properties and increases natural frequencies and critical buckling load and decreases bending parameter. It can be concluded that the adding CNTs leads to enhance stiffness of nanostructure. Also, the influence of adding CNTs are more significant in bending and buckling analysis rather than vibration.
(5) The natural frequencies and critical buckling load of theoretical method are higher than other methods because for industrial and hand layup method we cannot made a perfect composite beam with one hundred percent agreement by theoretical investigation. Also, the minimum deflection occurs for theoretical methods, in bending analysis.
(6) As can be seen, in this case the influence of applying more accurate processes to produce composite structures is more important than adding nano reinforcement particles.

Acknowledgments

The authors would like to thank the referees for their valuable comments. Also, they are thankful to the Iranian Nanotechnology Development Committee for their financial support, the University of Kashan for supporting this work by Grant No. 682561/3, and the ARKA SANAT COMPOSITE Company for financial support by Grant NO. 972018/1.

References

An, X., Khoo, B.C. and Cui, Y. (2017), "Nonlinear aeroelastic analysis of curved laminated composite panels", *Compos.*

Struct., **179**, 377-414.
Ansari, R., Torabi, J. and Shojaei, M.F. (2017), "Buckling and vibration analysis of embedded functionally graded carbon nanotubereinforced composite annular sector plates under thermal loading", *Compos. Part B*: *Eng*., **109**, 197-213.
Apuzzo, A., Barretta, R., Luciano, R., Marotti, D.E., Sciarra, F. and Penna, R. (2017), "Free vibrations of Bernoulli-Euler nano-beams by the stress-driven nonlocal integral model", *Compos. Part B*: *Eng*., **123**, 105-111.
Arani, A.G., BabaAkbar-Zarei, H., Pourmousa, P. and Eskandari, M. (2017a), "Investigation of free vibration response of smart sandwich micro-beam on Winkler---Pasternak substrate exposed to multi physical fields", *Microsyst. Technol*., **24**(7), 3045-3060**.**
Arani, A.G., Jafari, G.S. and Kolahchi, R. (2017b), "Nonlinear vibration analysis of viscoelastic micro nano‐composite sandwich plates integrated with sensor and actuator", *Microsyst. Technol*, **23**, 1509-1535.
Arefi, M. (2015), "Elastic solution of a curved beam made of functionally graded materials with different cross sections", Steel and Composite Structures., **18**(3), 659-672.
Arefi, M. and Zenkour, A.M. (2016), "A simplified shear and normal deformations nonlocal theory for bending of functionally graded piezomagnetic sandwich nanobeams in magneto-thermo-electric environment", *J. Sandw. Struct. Mater*., **18**(5), 624-651.
Arefi, M. and Zenkour, A.M. (2017a), "Size-dependent vibration and bending analyses of the piezomagnetic three-layer nanobeams", *Appl. Phys. A*, **123**(3), 202.
Arefi, M. and Zenkour, A.M. (2017b), "Vibration and bending analysis of a sandwich microbeam with two integrated piezo-magnetic face-sheets", *Compos. Struct*., **159**, 479-490.
Arefi, M. and Zenkour, A.M. (2017c), "Transient analysis of a three-layer microbeam subjected to electric potential", *Int. J. Smart Nano Mater*., **8**(1), 20-40.
Arefi, M. and Zenkour, A.M. (2018), "Size-dependent electro-elastic analysis of a sandwich microbeam based on higher-order sinusoidal shear deformation theory and strain gradient theory", *J. Intel. Mater. Syst. Struct*., **29**(7), 1394-1406.
Bandaru, A.K., Patel, S., Sachan, Y., Ahmad, S. and Alagirusamy, R. (2016), "Mechanical behavior of Kevlar/basalt reinforced polypropylene composites", *Compos. Part A*, **90**, 642-652.
Chen, D., Yang, J. and Kitipornchai, S. (2017), "Nonlinear vibration and postbuckling of functionally graded graphene reinforced porous nanocomposite beams", *Compos. Sci. Technol*., **142**, 235-245.
Ebrahimi, F. and Barati, M.R. (2017), "Size-dependent vibration analysis of viscoelastic nanocrystalline silicon nanobeams with porosities based on a higher order refined beam theory", *Compos. Struct*., **166**, 256-267.
Emam, S. and Eltaher, M.A. (2016), "Buckling and postbuckling of composite beams in hygrothermal environments", *Compos. Struct*., **152**, 665-675.
Emam, S.A. and Nayfeh, A.H. (2013), "Non-linear response of buckled beams to 1: 1 and 3: 1 internal resonances", *Non-Linear Mech*., **52**, 12-25.
Fereidoon, A., Eftekhari, D. and Yaghoobi, H. (2015), "Dynamic behavior of piezoelectric composite beams under moving loads", *J. Compos. Mater*., **50**, 899-916.
Filippi, M., Carrera, E. and Zenkour, A.M. (2015), "Static analyses of FGM beams by various theories and finite elements", Composites Part B: Engineering, **72**, 1-9.
Ganapathi, M. and Polit, O. (2017), "Dynamic characteristics of curved nanobeams using nonlocal higher-order curved beam theory", *Physica E*: *Low-dimens. Syst. Nanostruct*., **91**, 190-202.
Gholami, R. and Ansari, R. (2017), "A unified nonlocal nonlinear higher-order shear deformable plate model for postbuckling analysis of piezoelectric-piezomagnetic rectangular nanoplates with various edge supports", *Compos. Struct*., **166**, 202-218.
Gliszczyński, A. and Kubiak, T. (2017), "Load carrying capacity of thin-walled composite beams subjected to pure bending", *Thin-Wall. Struct*., **115**, 76-85.
Goncalves, B.R., Karttunen, A., Romanoff, J. and Reddy, J.N. (2017), "Buckling and free vibration of shear-flexible sandwich beams using a couple-stress-based finite element", *Compos. Struct*., **165**, 233-241.
Goswami, S. and Becker, W. (2015), "Analysis of sandwich plates with compressible core using layerwise refined plate theory and interface stress continuity", *J. Compos. Mater*., **50**, 201-217.
Hadi, M.N.S. and Yuan, J.S. (2017), "Experimental investigation of composite beams reinforced with GFRP I-beam and steel bars", *Constr. Build. Mater*., **144**, 462-474.
Jacob, G.C., Fellers, J.F., Simunovic, S. and Starbuck, J.M. (2002), "Energy Absorption in Polymer Composites for Automotive Crashworthiness", *J. Compos. Mater*., **36**, 813-850.
Jin, G., Yang, C. and Liu, Z. (2016), "Vibration and damping analysis of sandwich viscoelastic-core beam using Reddy's higher-order", *Compos. Struct*., **140**, 390-409.
Koochaki, G.R. (2011), "Free Vibration Analysis of Functionally Graded Beams", *Int. J. Mech. Aerosp. Ind. Mechatro. Manuf. Eng*., **5**, 514-517.
Lee, J.W. and Lee, J.Y. (2017), "Free vibration analysis of functionally graded Bernoulli-Euler beams using an exact transfer matrix expression", *Int. J. Mech. Sci*., **122**, 1-17.
Li, S.R., Cao, F.D. and Wan, Z.Q. (2013), "Bending solutions of FGM Timoshenko beams from those of the homogenous Euler–Bernoulli beams", *Appl. Math. Model*., **37**, 7077-7085.
Li, X., Li, L., Hu, Y., Ding, Z. and Deng, W. (2017), "Bending, buckling and vibration of axially functionally graded beams based on nonlocal strain gradient theory", *Compos. Struct*., **165**, 250-265.
Mehrabian, A., Haldar, A. and Reyes-Salazar, A. (2005), "Seismic response analysis of steel frames with post-North ridge connection", *Steel Compos. Struct*., *Int. J*., **5**(4), 271-287.
Mohammadimehr, M. and Mehrabi, M. (2017), "Stability and free vibration analysis of double-bonded micro composite sandwich cylindrical shells conveying fluid flow", *Appl. Math. Model*., **47**, 685-709.
Mohammadimehr, M. and Mostafavifar, M. (2016), "Free vibration analysis of sandwich plate with a transversely flexible core and FG-CNTs reinforced nanocomposite face sheets subjected to magnetic field and temperature-dependent material properties using SGT", *Compos. Part B*: *Eng*., **94**, 253-270.
Mohammadimehr, M. and Shahedi, S. (2016), "Nonlinear magneto-electro-mechanical vibration analysis of double-bonded sandwich Timoshenko microbeams based on MSGT using GDQM", *Steel Compos. Struct., Int. J*., **21**(1), 1-36.
Mohammadimehr, M., Navi, B.R. and Arani, A.G. (2015), "Free vibration of viscoelastic double-bonded polymeric nanocomposite plates reinforced by FG-SWCNTs using MSGT, sinusoidal shear deformation theory and meshless method", *Compos. Struct*., **131**, 654-671.
Mohammadimehr, M., Rostami, R. and Arefi, M. (2016), "Electro-elastic analysis of a sandwich thick plate considering FG core and composite piezoelectric layers on Pasternak foundation using TSDT", *Steel Compos. Struct., Int. J*., **20**(3), 513-543.
Mohammadimehr, M., Akhavan Alavi, S.M., Okhravi, S.V. and Edjtahed, S.H. (2017), "Free vibration analysis of micromagneto-electro-elastic cylindrical sandwich panel considering functionally graded carbon nanotube–reinforced nanocomposite face sheets, various circuit boundary conditions, and temperature-dependent material properties using high-order sandwich panel theory and modified strain gradient theory", *J. Int. Mater. Syst. Struct*., **29**(5), 863-882.
Mohammadimehr, M., Okhravi, S.V. and Akhavan Alavi, S.M.

(2018), "Free vibration analysis of magneto-electro-elastic cylindrical composite panel reinforced by various distributions of CNTs with considering open and closed circuits boundary conditions based on FSDT", *J. Vib. Control*, **24**(8), 1551-1569.

Naderi, A.A., Rahimi, G.H. and Arefi, M. (2014), "Influence of fiber paths on buckling load of tailored conical shells", *Steel Compos. Struct., Int. J.*, **16**(4), 375-387.

Nayak, A.K., Moy, S.S.J. and Shenoi, R.A. (2002), "Free vibration analysis of composite sandwich plates based on Reddy's higher-order theory", *Compos. Part B: Eng.*, **33**, 505-519.

Nguyen, T.T., Thang, P.T. and Lee, J. (2017), "Lateral buckling analysis of thin-walled functionally graded open-section beams", *Compos. Struct.*, **160**, 952-963.

Orun, A.E. and Guler, M.A. (2017), "Effect of hole reinforcement on the buckling behaviour of thin-walled beams subjected to combined loading", *Thin-Wall. Struct.*, **118**, 12-22.

Pagani, A. and Carrera, E. (2017), "Large-deflection and post-buckling analyses of laminated composite beams by Carrera Unified Formulation", *Compos. Struct.*, **170**, 40-52.

Petrone, G. and Meruane, V. (2017), "Mechanical properties updating of a non-uniform natural fibre composite panel by means of a parallel genetic algorithm", *Compos. Part A*, **94**, 226-233.

Piana, G., Lofrano, E., Manuello, A. and Ruta, G. (2017), "Natural frequencies and buckling of compressed non-symmetric thin-walled beams", *Thin-Wall. Struct.*, **111**, 189-196.

Scuciato, R.F., Carrer, J.A.M. and Mansur, W.J. (2017), "The time-dependent boundary element method formulation applied to dynamic analysis of Euler-Bernoulli beams: the linear θ method", *Eng. Anal. Bound. Elem.*, **79**, 98-109.

Shaat, M., Khorshidi, M.A., Abdelkefi, A. and Shariati, M. (2016), "Modeling and vibration characteristics of cracked nano-beams made of nanocrystalline materials", *Mech. Sci.*, **115**, 574-585.

Shao, D., Hu, S., Wang, Q. and Pang, F. (2017), "Free vibration of refined higher-order shear deformation composite laminated beams with general boundary conditions", *Compos. Part B: Eng.*, **108**, 75-90.

Sharma, K. and Shukla, M. (2014), "Three-phase carbon fiber amine functionalized carbon nanotubes epoxy composite: processing, characterisation, and multiscale modeling", *Nanomater.*, p. 2. DOI: http://dx.doi.org/10.1155/2014/837492

Vieira, R.F., Virtuoso, F.B.E. and Pereira, E.B.R. (2017), "Buckling of thin-walled structures through a higher order beam model", *Comput. Struct.*, **180**, 104-116.

Wattanasakulpong, N., Prusty, B.G., Kelly, D.W. and Hoffman, M. (2012), "Free vibration analysis of layered functionally graded beams with experimental validation", *J. Mater. Des.*, **36**, 182-190.

Xu, X., Han, Q. and Chu, F. (2017), "Nonlinear vibration of a rotating cantilever beam in a surrounding magnetic field", *Int. J. Non-Linear Mech.*, **95**, 59-72.

Yang, L., Fan, T., Yang, L., Han, X. and Chen, Z. (2017), "Bending of functionally graded nanobeams incorporating surface effects based on Timoshenko beam model", *Theor. Appl. Mech. Lett.*, **7**(3), 152-158.

Zamani, H.A., Bodaghi, M., Aghdam, M.M. and Salehi, M. (2014), "Accurate damping analysis of viscoelastic composite beams and plates on suppressive foundation", *J. Compos. Mater.*, **49**, 2187-2202.

Zhang, Z.J., Han, B., Zhang, Q.C. and Jin, F. (2017), "Free vibration analysis of sandwich beams with honeycomb-corrugation hybrid cores", *Compos. Struct.*, **171**, 335-344.

Zhong, Y., Wu, G., Ren, H. and Jiang, Z. (2017), "Bending properties evaluation of newly designed reinforced bamboo scrimber composite beams", *Constr. Build. Mater.*, **143**, 61-70.

Zhu, X., Wang, Y. and Dai, H.H. (2017), "Buckling analysis of Euler–Bernoulli beams using Eringen's two-phase nonlocal model", *Int. J. Eng. Sci.*, **116**, 130-140.

CC

Appendix A

By substituting the Eqs. (29), (32) and (33) in the Hamilton's principle, the equations of the motion for the nanocomposite beam are completely defined in Appendix A.

$$
\begin{aligned}
&\frac{4}{3}\frac{bI_3\alpha_3\frac{\partial}{\partial x}\left(\frac{\partial}{\partial t}\left(\frac{\partial}{\partial t}w_0(x,t)\right)\right)}{h^2}\\
&-\frac{4}{3}\frac{bI_3\alpha_3\frac{\partial}{\partial t}\left(\frac{\partial}{\partial t}\psi_0(x,t)\right)}{h^2}\\
&+\frac{4}{3}\frac{bB_3\alpha_3\frac{\partial}{\partial x}\left(\frac{\partial}{\partial x}\psi_0(x,t)\right)}{h^2}\\
&+\frac{4}{3}\frac{bB_3\alpha_3\frac{\partial}{\partial x}\left(\frac{\partial}{\partial x}\left(\frac{\partial}{\partial x}w_0(x,t)\right)\right)}{h^2}\\
&-bI_0\frac{\partial}{\partial t}\left(\frac{\partial}{\partial t}u_0(x,t)\right)-bB_0\frac{\partial}{\partial x}\left(\frac{\partial}{\partial x}u_0(x,t)\right)\\
&+bB_1\alpha_1\frac{\partial}{\partial x}\left(\frac{\partial}{\partial x}\left(\frac{\partial}{\partial x}w_0(x,t)\right)\right)\\
&-bB_1\alpha_2\frac{\partial}{\partial x}\left(\frac{\partial}{\partial x}\psi_0(x,t)\right)\\
&-bI_1\alpha_1\frac{\partial}{\partial x}\left(\frac{\partial}{\partial t}\left(\frac{\partial}{\partial t}w_0(x,t)\right)\right)\\
&+bI_1\alpha_2\frac{\partial}{\partial t}\left(\frac{\partial}{\partial t}\psi_0(x,t)\right)=0
\end{aligned}
\tag{A1}
$$

$$
\begin{aligned}
&-\frac{16}{9}\frac{bI_6\alpha_3^2\frac{\partial}{\partial x}\left(\frac{\partial}{\partial x}\left(\frac{\partial}{\partial t}\left(\frac{\partial}{\partial t}w_0(x,t)\right)\right)\right)}{h^4}\\
&-\frac{16}{9}\frac{bI_6\alpha_3^2\frac{\partial}{\partial x}\left(\frac{\partial}{\partial t}\left(\frac{\partial}{\partial t}\psi_0(x,t)\right)\right)}{h^4}\\
&+\frac{16}{9}\frac{bB_5\alpha_3^2\frac{\partial}{\partial x}\left(\frac{\partial}{\partial x}\left(\frac{\partial}{\partial x}\left(\frac{\partial}{\partial x}w_0(x,t)\right)\right)\right)}{h^4}\\
&+bC_0\alpha_1\alpha_2\frac{\partial}{\partial x}\psi_0(x,t)+\frac{4bC_2\alpha_3\frac{\partial}{\partial x}\psi_0(x,t)}{h^2}\\
&-\frac{16bC_4\alpha_3^2\frac{\partial}{\partial x}\left(\frac{\partial}{\partial x}w_0(x,t)\right)}{h^4}+\frac{8bC_2\alpha_3\frac{\partial}{\partial x}\left(\frac{\partial}{\partial x}w_0(x,t)\right)}{h^2}\\
&-\frac{16bC_4\alpha_3^2\frac{\partial}{\partial x}\psi_0(x,t)}{h^4}
\end{aligned}
\tag{A2}
$$

$$
\begin{aligned}
&+\frac{4}{3}\frac{bI_3\alpha_3\frac{\partial}{\partial x}\left(\frac{\partial}{\partial t}\left(\frac{\partial}{\partial t}u_0(x,t)\right)\right)}{h^2}\\
&+bI_2\alpha_1\alpha_2\frac{\partial}{\partial x}\left(\frac{\partial}{\partial t}\left(\frac{\partial}{\partial t}\psi_0(x,t)\right)\right)\\
&-bB_2\alpha_1\alpha_2\frac{\partial}{\partial x}\left(\frac{\partial}{\partial x}\left(\frac{\partial}{\partial x}\psi_0(x,t)\right)\right)\\
&-\frac{4}{3}\frac{bB_3\alpha_3\frac{\partial}{\partial x}\left(\frac{\partial}{\partial x}\left(\frac{\partial}{\partial x}u_0(x,t)\right)\right)}{h^2}\\
&+\frac{16}{9}\frac{bB_5\alpha_3^2\frac{\partial}{\partial x}\left(\frac{\partial}{\partial x}\left(\frac{\partial}{\partial x}\psi_0(x,t)\right)\right)}{h^4}\\
&-bI_2\alpha_1^2\frac{\partial}{\partial x}\left(\frac{\partial}{\partial x}\left(\frac{\partial}{\partial t}\left(\frac{\partial}{\partial t}w_0(x,t)\right)\right)\right)\\
&+bI_1\alpha_1\frac{\partial}{\partial x}\left(\frac{\partial}{\partial t}\left(\frac{\partial}{\partial t}u_0(x,t)\right)\right)\\
&-bB_1\alpha_1\frac{\partial}{\partial x}\left(\frac{\partial}{\partial x}\left(\frac{\partial}{\partial x}u_0(x,t)\right)\right)\\
&+bB_2\alpha_1^2\frac{\partial}{\partial x}\left(\frac{\partial}{\partial x}\left(\frac{\partial}{\partial x}\left(\frac{\partial}{\partial x}w_0(x,t)\right)\right)\right)\\
&-bC_0\alpha_1^2\frac{\partial}{\partial x}\left(\frac{\partial}{\partial x}w_0(x,t)\right)-bC_0\alpha_2\frac{\partial}{\partial x}\psi_0(x,t)\\
&+2bC_0\alpha_1\frac{\partial}{\partial x}\left(\frac{\partial}{\partial x}w_0(x,t)\right)+bI_0\frac{\partial}{\partial t}\left(\frac{\partial}{\partial t}w_0(x,t)\right)\\
&-bC_0\frac{\partial}{\partial x}\left(\frac{\partial}{\partial x}w_0(x,t)\right)-f_z(x)\\
&-\frac{4}{3}\frac{bI_4\alpha_1\alpha_3\frac{\partial}{\partial x}\left(\frac{\partial}{\partial t}\left(\frac{\partial}{\partial t}\psi_0(x,t)\right)\right)}{h^2}\\
&+\frac{8}{3}\frac{bB_4\alpha_1\alpha_3\frac{\partial}{\partial x}\left(\frac{\partial}{\partial x}\left(\frac{\partial}{\partial x}\left(\frac{\partial}{\partial x}w_0(x,t)\right)\right)\right)}{h^2}\\
&-\frac{4}{3}\frac{bB_4\alpha_2\alpha_3\frac{\partial}{\partial x}\left(\frac{\partial}{\partial x}\left(\frac{\partial}{\partial x}\psi_0(x,t)\right)\right)}{h^2}\\
&+\frac{4}{3}\frac{bB_4\alpha_1\alpha_3\frac{\partial}{\partial x}\left(\frac{\partial}{\partial x}\left(\frac{\partial}{\partial x}\psi_0(x,t)\right)\right)}{h^2}\\
&-\frac{8bC_2\alpha_1\alpha_3\frac{\partial}{\partial x}\left(\frac{\partial}{\partial x}w_0(x,t)\right)}{h^2}\\
&+\frac{4bC_2\alpha_2\frac{\partial}{\partial x}\psi_0(x,t)}{h^2}-\frac{4bC_1\alpha_3\frac{\partial}{\partial x}\psi_0(x,t)}{h^2}
\end{aligned}
\tag{A2}
$$

$$-\frac{8}{3}\frac{bI_4\alpha_1\alpha_3\frac{\partial}{\partial x}\left(\frac{\partial}{\partial x}\left(\frac{\partial}{\partial t}\left(\frac{\partial}{\partial t}w_0(x,t)\right)\right)\right)}{h^2}$$
$$+\frac{4}{3}\frac{bI_4\alpha_2\alpha_3\frac{\partial}{\partial x}\left(\frac{\partial}{\partial t}\left(\frac{\partial}{\partial t}\psi_0(x,t)\right)\right)}{h^2}=0 \quad \text{(A2)}$$

$$\frac{16}{9}\frac{bI_6\alpha_3^2\frac{\partial}{\partial x}\left(\frac{\partial}{\partial t}\left(\frac{\partial}{\partial t}w_0(x,t)\right)\right)}{h^4}$$
$$+bB_2\alpha_1\alpha_2\frac{\partial}{\partial x}\left(\frac{\partial}{\partial x}\left(\frac{\partial}{\partial x}w_0(x,t)\right)\right)$$
$$+\frac{4}{3}\frac{bB_3\alpha_3\frac{\partial}{\partial x}\left(\frac{\partial}{\partial x}u_0(x,t)\right)}{h^2}$$
$$-\frac{16}{9}\frac{bB_5\alpha_3^2\frac{\partial}{\partial x}\left(\frac{\partial}{\partial x}\psi_0(x,t)\right)}{h^4}$$
$$+\frac{16}{9}\frac{bI_6\alpha_3^2\frac{\partial}{\partial t}\left(\frac{\partial}{\partial t}\psi_0(x,t)\right)}{h^4}-\frac{4bC_2\alpha_3\frac{\partial}{\partial x}w_0(x,t)}{h^2}$$
$$-\frac{16}{9}\frac{bB_5\alpha_3^2\frac{\partial}{\partial x}\left(\frac{\partial}{\partial x}\left(\frac{\partial}{\partial x}w_0(x,t)\right)\right)}{h^4}$$
$$-bC_0\alpha_1\alpha_2\frac{\partial}{\partial x}w_0(x,t)+\frac{16bC_4\alpha_3^2\frac{\partial}{\partial x}\psi_0(x,t)}{h^4}$$
$$+\frac{16bC_4\alpha_3^2\frac{\partial}{\partial x}w_0(x,t)}{h^4}-\frac{4}{3}\frac{bI_3\alpha_3\frac{\partial}{\partial t}\left(\frac{\partial}{\partial t}u_0(x,t)\right)}{h^2} \quad \text{(A3)}$$
$$-bI_2\alpha_1\alpha_2\frac{\partial}{\partial x}\left(\frac{\partial}{\partial t}\left(\frac{\partial}{\partial t}w_0(x,t)\right)\right)$$
$$+\frac{8}{3}\frac{bB_4\alpha_2\alpha_3\frac{\partial}{\partial x}\left(\frac{\partial}{\partial x}\psi_0(x,t)\right)}{h^2}$$
$$+\frac{4}{3}\frac{bB_4\alpha_2\alpha_3\frac{\partial}{\partial x}\left(\frac{\partial}{\partial x}\left(\frac{\partial}{\partial x}w_0(x,t)\right)\right)}{h^2}$$
$$-\frac{8bC_2\alpha_2\alpha_3\psi_0(x,t)}{h^2}-\frac{4bC_2\alpha_2\alpha_3\frac{\partial}{\partial x}w_0(x,t)}{h^2}$$
$$+\frac{4bC_2\alpha_1\alpha_3\frac{\partial}{\partial x}w_0(x,t)}{h^2}$$
$$+\frac{4}{3}\frac{bI_4\alpha_1\alpha_3\frac{\partial}{\partial x}\left(\frac{\partial}{\partial t}\left(\frac{\partial}{\partial t}w_0(x,t)\right)\right)}{h^2}$$
$$-\frac{8}{3}\frac{bI_4\alpha_2\alpha_3\frac{\partial}{\partial t}\left(\frac{\partial}{\partial t}\psi_0(x,t)\right)}{h^2}$$
$$-\frac{4}{3}\frac{bI_4\alpha_2\alpha_3\frac{\partial}{\partial x}\left(\frac{\partial}{\partial t}\left(\frac{\partial}{\partial t}w_0(x,t)\right)\right)}{h^2}-$$
$$-\frac{4}{3}\frac{bB_4\alpha_1\alpha_3\frac{\partial}{\partial x}\left(\frac{\partial}{\partial x}\left(\frac{\partial}{\partial x}w_0(x,t)\right)\right)}{h^2}$$
$$-bB_1\alpha_2\frac{\partial}{\partial x}\left(\frac{\partial}{\partial x}u_0(x,t)\right)-bB_2\alpha_2^2\frac{\partial}{\partial x}\left(\frac{\partial}{\partial x}\psi_0(x,t)\right) \quad \text{(A3)}$$
$$+bC_0\alpha_2^2\psi_0(x,t)+bC_0\alpha_2\frac{\partial}{\partial x}w_0(x,t)$$
$$+bI_2\alpha_2^2\frac{\partial}{\partial t}\left(\frac{\partial}{\partial t}\psi_0(x,t)\right)+bI_1\alpha_2\frac{\partial}{\partial t}\left(\frac{\partial}{\partial t}u_0(x,t)\right)=0$$

where B_i, C_i and I_i parameters are defined as follows

$$B_i=\int_{-0.5h}^{0.5h}Q_{11}(z)z^i dz \qquad i=0,1,2,3,4,6 \quad \text{(A4)}$$

$$C_i=\int_{-0.5h}^{0.5h}Q_{22}(z)z^i dz \qquad i=0,2,4 \quad \text{(A5)}$$

$$I_i=\int_{-0.5h}^{0.5h}\rho(z)z^i dz \qquad i=0,1,2,3,4,6 \quad \text{(A6)}$$